Chapter 8

Investigation of Drying Mechanism of Solids Using Wind Tunnel

Abdulaziz Almubarak

Additional information is available at the end of the chapter

http://dx.doi.org/10.5772/54322

1. Introduction

Drying of solids provides a technical challenge due to the presence of complex interactions between the simultaneous processes of heat and mass transfer, both on the surface and within the structure of the materials being dried. Internal moisture flow can occur by a complex mechanism depending on the structure of the solid body, moisture content, temperature and pressure in capillaries and pores. External conditions such as temperature, humidity, pressure, the flow velocity of the drying medium and the area of exposed surface also have a great effect on the mechanisms of drying.

Theoretical and experimental studies [1-6] reported the forced convection heat and mass transfer across different shapes. Most of these studies have considered a heated solid surface with a uniform surface temperature. However, this situation is not the same as in the drying process, where heat and mass transfer occurs simultaneously and the interfacial temperature and moisture content vary during the drying.

Evaporation from a flat plate surface to a laminar boundary layer was theoretically analyzed [7]. It was calculated distributions of the interfacial temperature and local Nusselt and Sherwood numbers for a parallel flow where both Prandtl and Schmidt numbers are unity. A conclusion stated that the characteristics of heat and mass transfer are highly conjugated and significantly influenced by the temperature dependency of vapor-liquid equilibrium, the magnitude of the latent heat of the phase change, and the thermal conductance of the flat plate. The work needs to be extended for the case of unsteady state conditions and to be repeated for a drying bed.

The variation in the surface temperature for a flat bed of a capillary porous material was discussed in [8]. The authors presented graphs that show an increase in surface temperature

from the leading edge of the flat plate during the periods of drying. They also showed graphs in which the surface temperature decreased. In general, a physical meaning for that contradiction was needed to be considered.

As in [9], Jomaa *et al.* presented a simulation of the high-temperature drying of a paste in a scaled-up wind tunnel. They attempted to study the influence of the local air flow and thermal radiation on the drying behaviour of the product. A rapid air velocity (8 m s^{-1}) was used in the experiment, and an empirical model was derived to predict temperature and solvent content along the conveyer belt. Comparison of the experimental results with those predicted ones by the model showed a satisfactory agreement.

Evaporation of a pure liquid droplet has been widely studied both theoretically and experimentally [10-14]. However, in spray dryers and droplet drying applications, the droplets always consisted of multi-component mixtures of liquids and sometimes dissolved solids, forming a complicated multiphase composition. This makes analyzing heat and mass transfer processes more difficult. This effect is attributed to the presence of various components that vaporize at different rates, giving rise to a gradient in concentration in the liquid and vapor phase. In addition, a solid crust forms at the outer surface of droplet which acts as a resistance to heat and mass transfer processes.

Various experimental techniques have been used [15-19] to study the mechanisms of drying for a single droplet containing dissolved solids. The droplet was suspended freely from the end of a stable nozzle fixed in a wind tunnel. Air flow was hitting the droplet from one side causing a significant disturbance to the shape of droplet. Therefore, there was some difficulty in recording the weight and temperature of the droplet. The transferred heat conduction to the droplet by the nozzle was another problem.

Cheong *et al.* [20] proposed a mathematical model to predict core temperature for drying a free suspended droplet against time. Reasonable agreement was obtained between the predicted and the experimental results at an air temperature of 20ºC. However, the predicted temperature was less accurate at higher temperatures (50ºC and 70ºC); the model was not applicable for cases at high air temperatures.

A mathematical model was modified in [21], taking into account the droplet shrinkage. The droplet was assumed first to undergo sensible heating with no mass change. The model showed that temperature distribution within the droplet cannot be ignored even for a small diameter droplet of 200 μm.

Wind tunnel definitely is considered one of the best tools to investigate and to study the role of boundary layer and the mechanisms of drying process. The most important variables in any drying process such as air flow, temperature and humidity are usually easy to be controlled inside the wind tunnel. In the current study, through an experimental work and mathematical approach, we attempt to understand the role of the boundary layer on the interface behavior and the drying mechanisms for various materials of a flat plate surface and a single droplet shape.

http://dx.doi.org/10.5772/54322

2. Boundary layer over a flat plate surface

A boundary layer developed over a flat-plate surface plays a great role in the mechanisms of convective drying. Very little work has been done on the conjugated problem of heat and mass transfer during a flow over a drying bed. In this paper, through an experimental and mathematical approach, we attempt to understand the role of the thermal boundary layer on the interface behavior and the drying mechanisms for porous mediums. Beds of desert sand, beach sand and glass beads were subjected to forced convective drying in a scaled-up wind tunnel.

A laboratory-scale dryer designed for this work is shown in Figure 1. The apparatus consists of wind tunnel, molecular-sieve air dryer, 3 KW air heater and a fan. Through the wind tunnel a controlled flow of hot, dry air, with an average velocity of 1 m s^{-1}, was passed over a sample mounted flush with the tunnel floor. The last section of the wind tunnel (converging section) was designed to be opened easily for installation of the test bed.

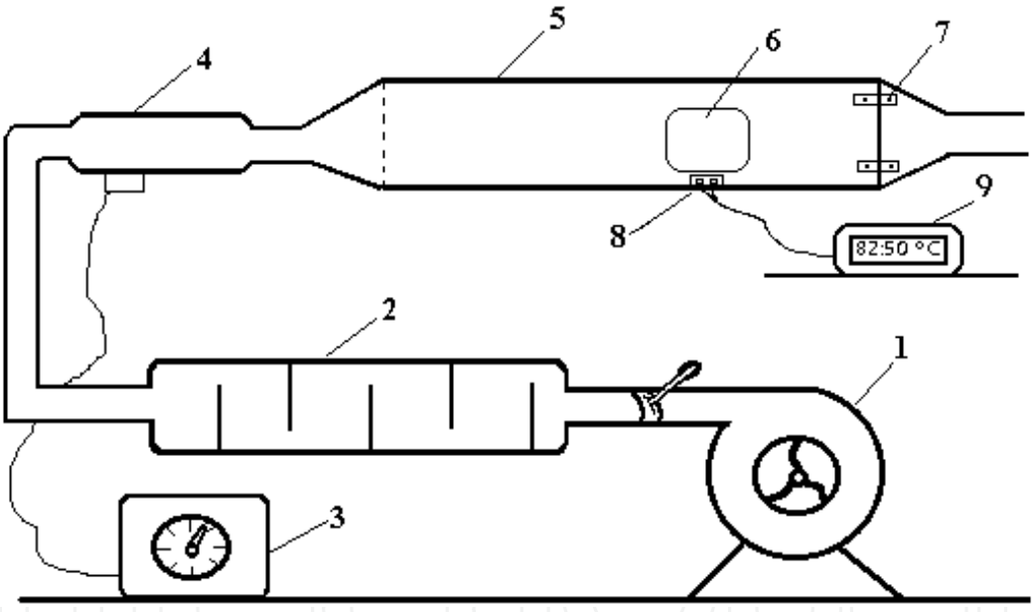

Figure 1. Experimental apparatus composed of: 1. fan; 2. molecular-sieve air dryer; 3. voltage regulator; 4. air heater; 5. wind tunnel; 6. observation port; 7. joint; 8. thermocouple socket; 9. thermocouple selector.

A glass tray (100 cm x 36 cm x 2.5 cm) attached to a flat metal plate was especially designed for this study. The top surface of the glass tray was at the same level of the metal plate that formed the floor of the wind tunnel. The sides and the bottom of the tray are insulated with neoprene rubber to minimize heat transfer *via* the glass wall. Figure 2 shows both the wind tunnel and the glass tray.

Ten thermocouples were inserted from one side of the tray to facilitate measurement of surface temperature distribution along the bed. At the same side of the tray, another ten ther-

mocouples were inserted but at lower depth, 2.2 cm from the surface, to measure the bottom temperature distribution.

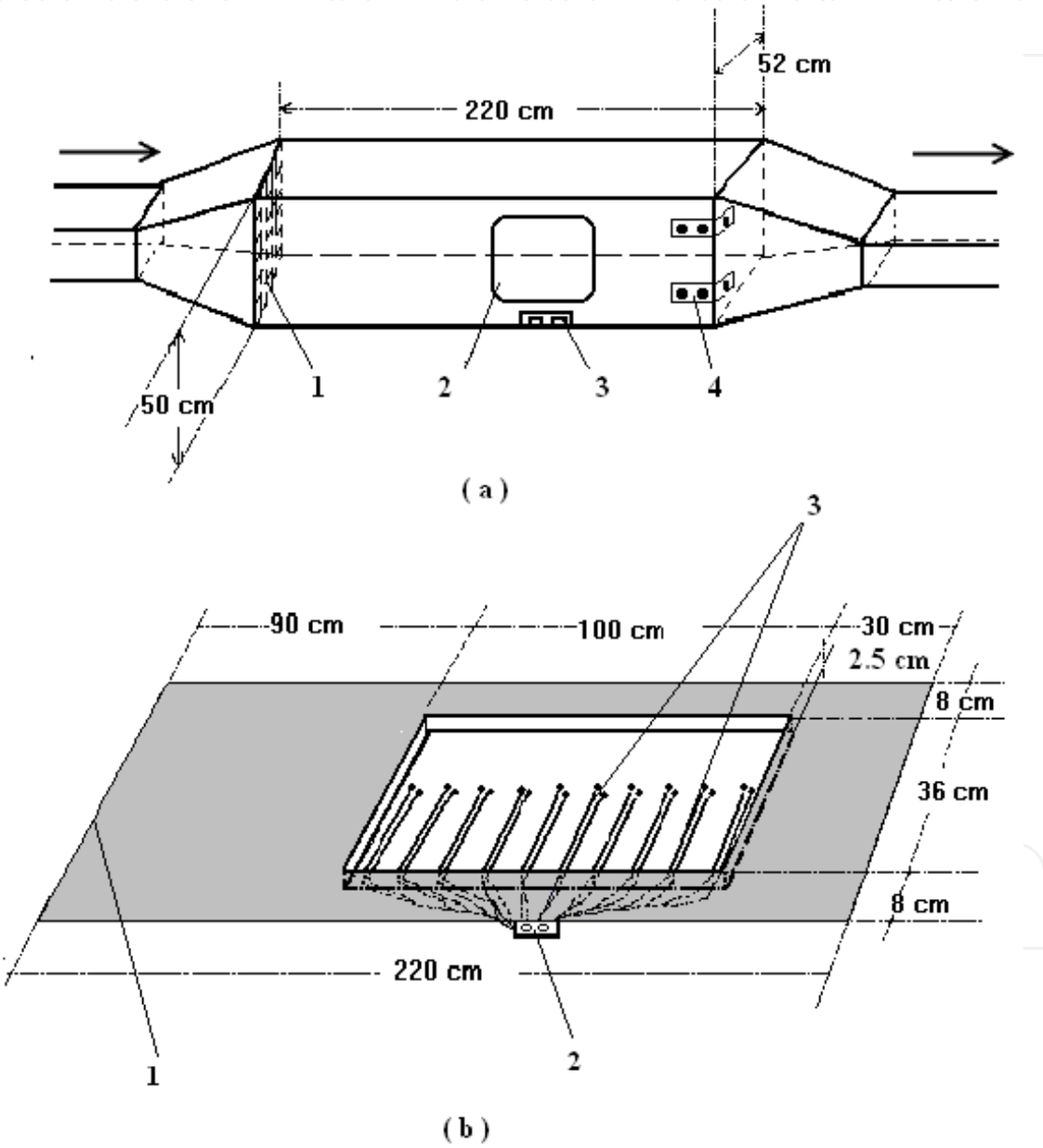

Figure 2. Details of (a) Wind tunnel: 1. smoothing grid; 2. observation port; 3.thermocouple socket; 4. joint, (b) Glass tray (clear) and flat plate (gray): 1. the leading edge; 2. thermocouple socket; 3. thermocouples.

http://dx.doi.org/10.5772/54322

The experiment was initiated by switching on the centrifugal fan and then the electric air heater. The voltage regulator was adjusted to provide the desired air temperature. The air temperature was monitored until it reached a steady state. This state was normally required 1 - 2 hours to be achieved.

When the apparatus achieved a constant air temperature, the drying process was commenced. The metal plate and the glass tray, containing the sample, were placed carefully inside the tunnel, allowing the hot air to pass over the surface of the bed. The initial readings of time and temperature were then registered immediately. During the experiment, temperature distributions were measured at intervals of approximately 20 minutes. The temperature at each distance was measured by using the thermocouple selector and registered with an accuracy ± 0.05ºC.

Two types of sand were subjected to the drying process. The first type was a fine sand of average grain size 220 μm diameter, with a moisture content of 0.17 kg kg^{-1}, taken from the desert of Kuwait, Burgan (N 28º 44 00 E 047º 42 00). The nature of the desert sand is usually fine and dry. The other type of sand was a beach sand of average grain size 300 μm diameter and 0.24 kg kg^{-1} moisture content, taken from the north coast of Kuwait, Bobiyan Island (N 29º 46 00 E 048º 22 00). The north coast is a place where the Shatt Al-Arab River (Iraq) falls into the Arabian Gulf. This makes the coast more muddy and less saline than the south coast. In addition, the beach sand contains a lot of small shells of various shapes. Glass beads of 400 μm diameter and 0.2 kg kg^{-1} initial moisture content were also selected, for test as a porous medium for comparison. The bed of glass beads is considered a typical sample for drying experiments, since the sizes of the beads are almost identical. The two types of sand and the glass beads beds are good examples for testing drying processes.

2.1. Results

A bed of the desert sand was subjected to forced convective drying at 84 ºC. The wet-bulb temperature of the air was 35.5 ºC. The resulting surface temperature vs. time at different distances from the leading is shown in Figure 3, which demonstrates clearly the stages of the drying process; i.e. the pre-constant rate period, the constant rate period, and the falling rate period.

The temperature of the bed rose from ambient temperature 23ºC to a steady value at time = 70 minute. This initial period, termed the pre-constant rate period, is usually short. The surface temperatures remained constant for a period of 140 minutes, indicating the constant rate period. The surface temperature at the distance x=1cm, from the leading edge was 36 ºC. This temperature was greater than that at x=50 cm and at x= 100 cm by 1 ºC and 2 ºC respectively. The surface temperatures were close to the wet-bulb temperature.

During the constant rate period, the surface of the solid is so wet that a continuous film of water exists on the drying surface. This water is entirely unbound water and exerts a vapour pressure equal to that of pure water at the same temperature. The rate of moisture movement within the solid is sufficient to maintain a saturated condition at the surface.

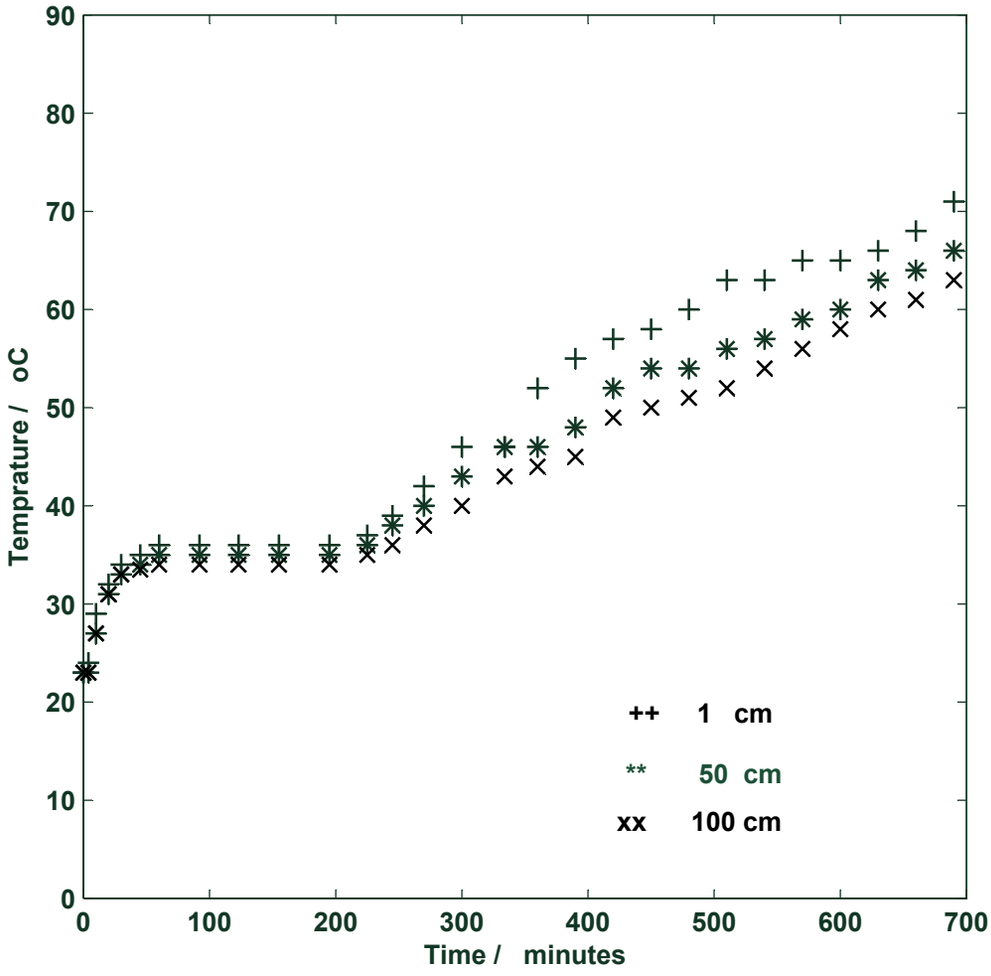

Figure 3. Temperature distribution profile of the surface for the desert sand bed.

At a specific point, t = 240 minutes, the surface temperature at all positions rose gradually, indicating the end of the constant-rate period and the beginning of the falling-rate period. In the falling-rate period, there was insufficient water on the surface to maintain a continuous film. The entire surface was no longer wetted and dry patches began to form. The surface temperature continued to rise for a longer time until it approximated to the air temperature. A thin dried layer appeared on the entire surface.

The temperatures at the surface and the bottom at different distances from the leading edge are shown in Figure 4. The profiles show that when the surface became dry, the bottom remained wet at a constant temperature for a longer time than that for the surface. During the falling-rate periods a receding evaporation front divided the system into a hotter, dry zone near the surface and a wet zone towards the bottom of the sample [22]. The evaporation plane receded from the surface toward the bottom. The temperatures then rose quickly when the dry zone extended throughout the bed.

http://dx.doi.org/10.5772/54322

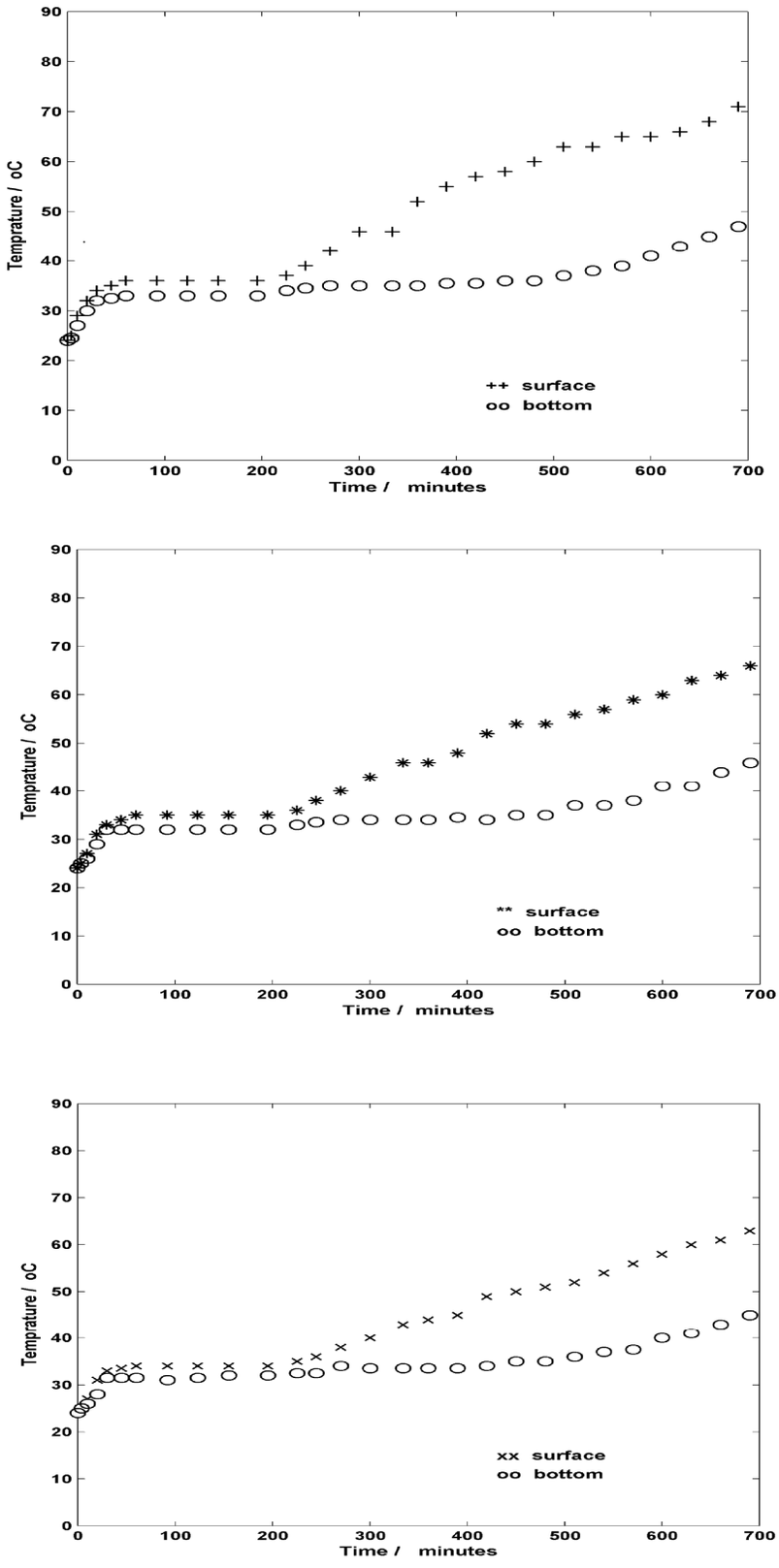

Figure 4. Temperatures of surface and bottom for the desert sand bed at distance of 1 cm, 50 cm and 100 cm from the leading edge, respectively, from the top.

A bed of the beach sand was dried at an air temperature of 83 °C. The wet bulb temperature was 35 °C. The temperature distribution profile at different distances from the leading edge is shown in Figure 5. The stages of the drying process can easily be recognized from the temperature profile. However, the surface temperature took longer to approach to the air temperature.

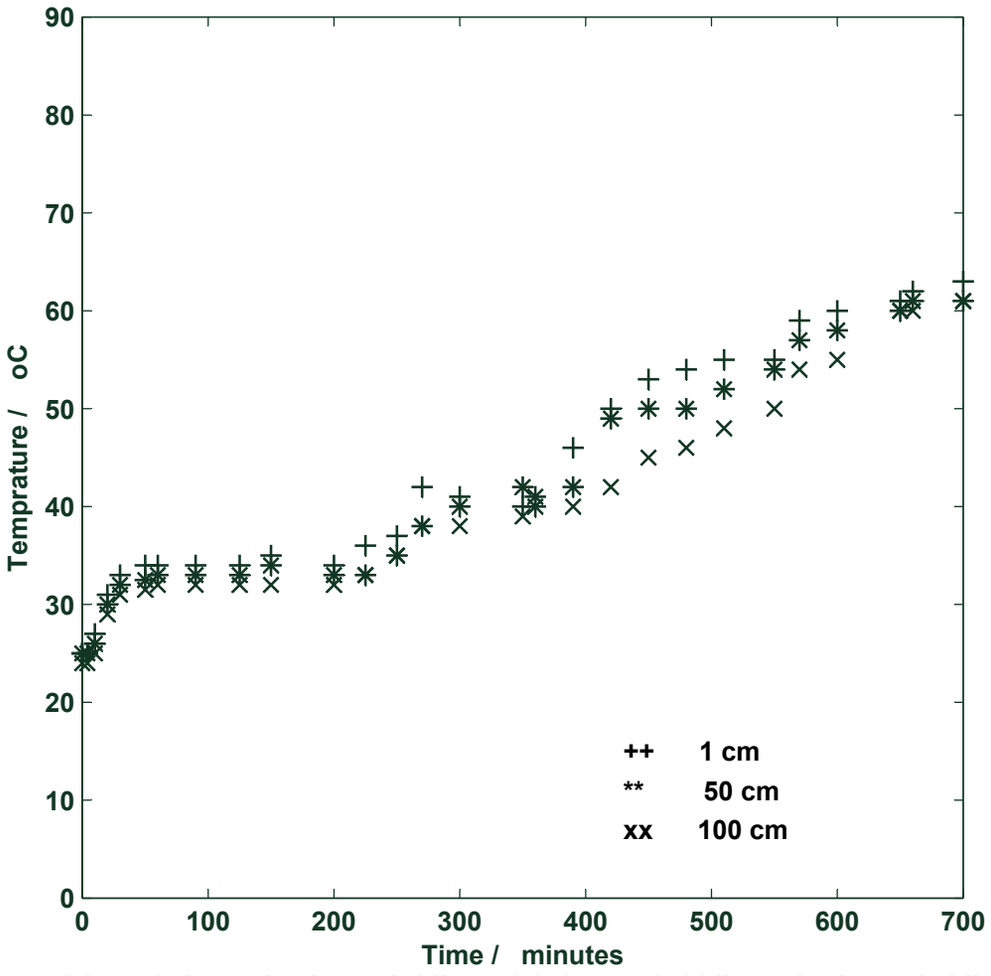

Figure 5. Temperature distribution profile of the surface for the beach sand bed).

Figure 6 shows the surface and the bottom temperatures at distances from the leading edge of 1 cm, 50 cm 100 cm, respectively. It can be seen that the surface and bottom temperatures increased rapidly at some times and decreased others. Also, the temperature profile did not increase gradually like that of the desert sand. This can be attributed to the nature of the beach sand, which comprises different types of small shells of various shapes, and contain tiny hollows. The trapped water in these hollows forms small bubbles which can explode with increasing temperature. Therefore the temperature of the bed changes suddenly at such times. The temperature at the bottom of the bed indicated it remained wet during the falling-rate period.

http://dx.doi.org/10.5772/54322

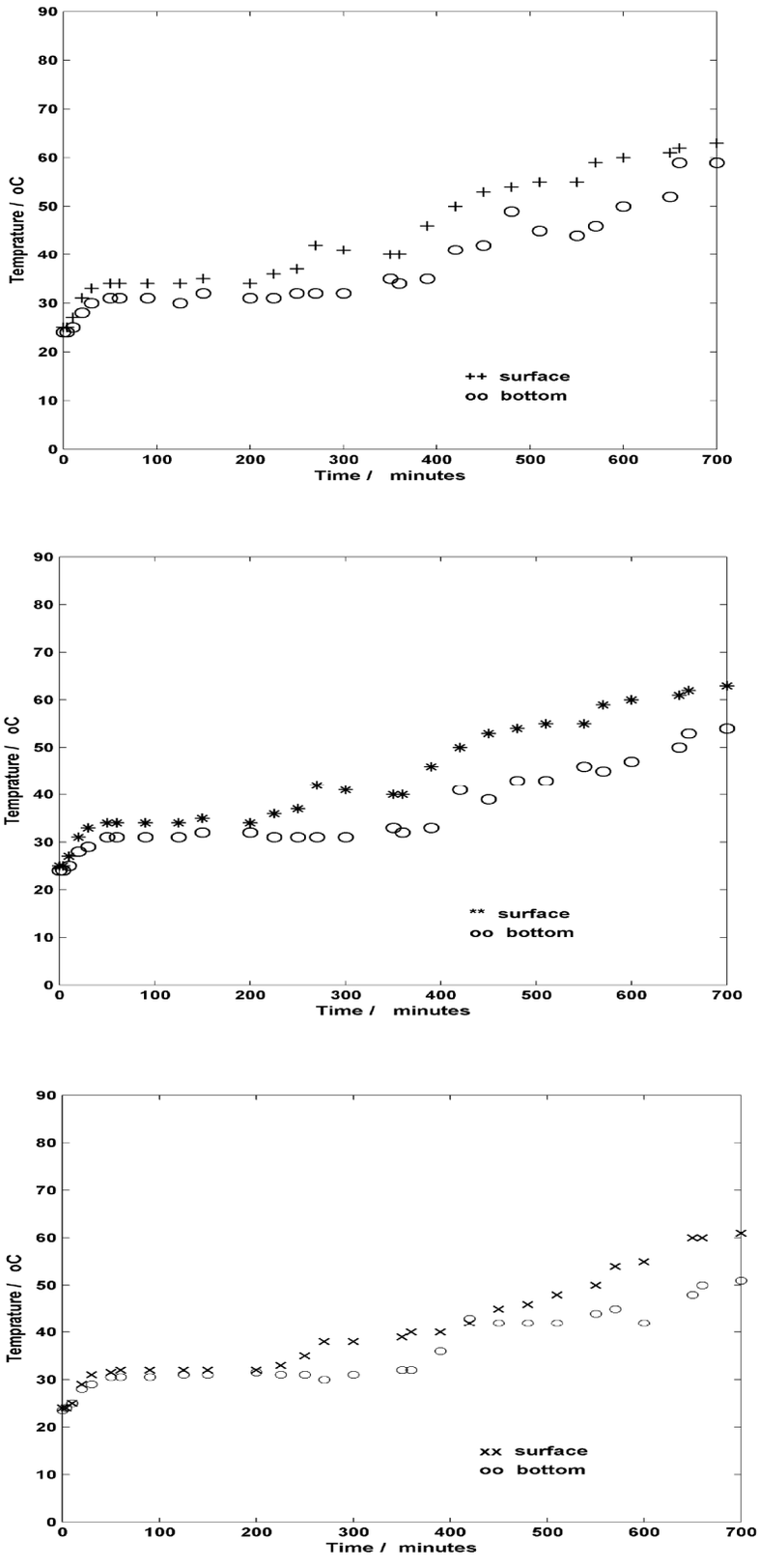

Figure 6. Temperatures of surface and bottom for the beach sand bed at distance of 1 cm, 50 cm and 100 cm from the leading edge, respectively, from the top.

A similar investigation was carried out for a bed of the glass beads at an air temperature of 84 °C. The wet bulb temperature was 37 °C. Figure 7 shows temperature versus time at different distances from the leading edge of the bed surface. The temperature distribution profile again illustrates clearly the stages of the drying process. The results for the surface and bottom temperatures for the glass beads were almost similar to those for the desert sand as shown in Figure 4.

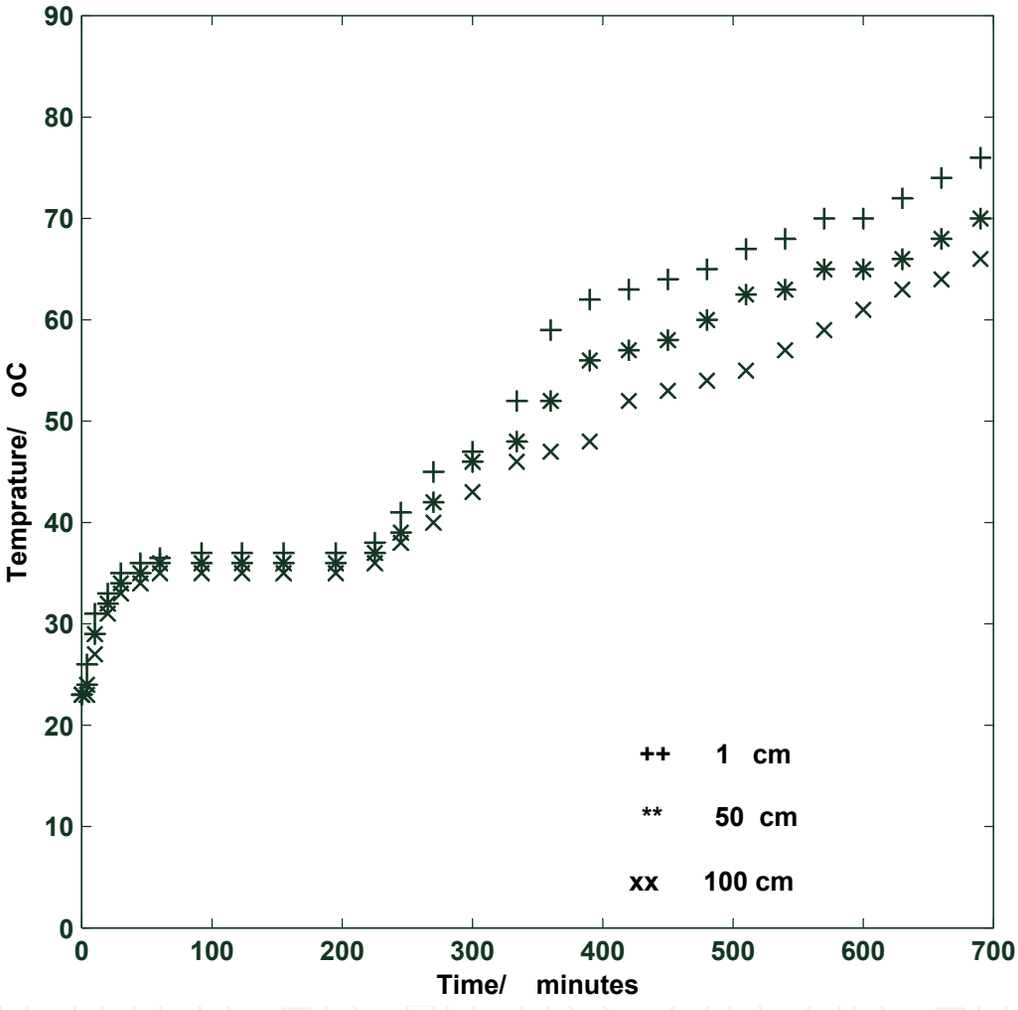

Figure 7. Temperature distribution profile of the surface for the glass-bead bed.

2.2. Discussion

A thin film adjacent to the surface always exists when a forced flow passes over a flat plate and forms what is called a hydrodynamic boundary layer. The influence of the surface temperature reaches deeper into the fluid, thus causing the formation of a thermal boundary layer. It is well known, the thickness of the thermal boundary layer increases with increasing distance from the leading edge. This layer is affected by the geometry of the system, roughness of the surface and the fluid properties.

http://dx.doi.org/10.5772/54322

For the case in which the heated section is preceded by an unheated straight length, the local Nusselt number (Nu_x) is represented in [23-25] as:

$$\mathrm{Nu_x} = \frac{\mathrm{h\,x}}{\mathrm{k}} = \frac{0.323(\mathrm{Re_x})^{0.5}(\mathrm{Pr})^{1/3}}{[1-(\mathrm{x_o}/\mathrm{x})^{3/4}]^{1/3}} \tag{1}$$

where Re_x is Reynolds number with respect to length and x is the length of the flat plate in (m).

Figure 8 shows a plot of variation in the local heat transfer coefficient versus the distance from the leading edge. The plot indicates that the values of the coefficient decreased significantly when x increased from the leading edge, and then it remains virtually constant for large x values. A plot of variation of the mass transfer coefficient could be expected to be almost similar to that in Figure 8 because of the similarity in the transport coefficient equations. This result with the concept of the boundary layer thickness demonstrates that resistance to heat and mass transfer to, or from, the bed increases with increasing the distance from the leading edge.

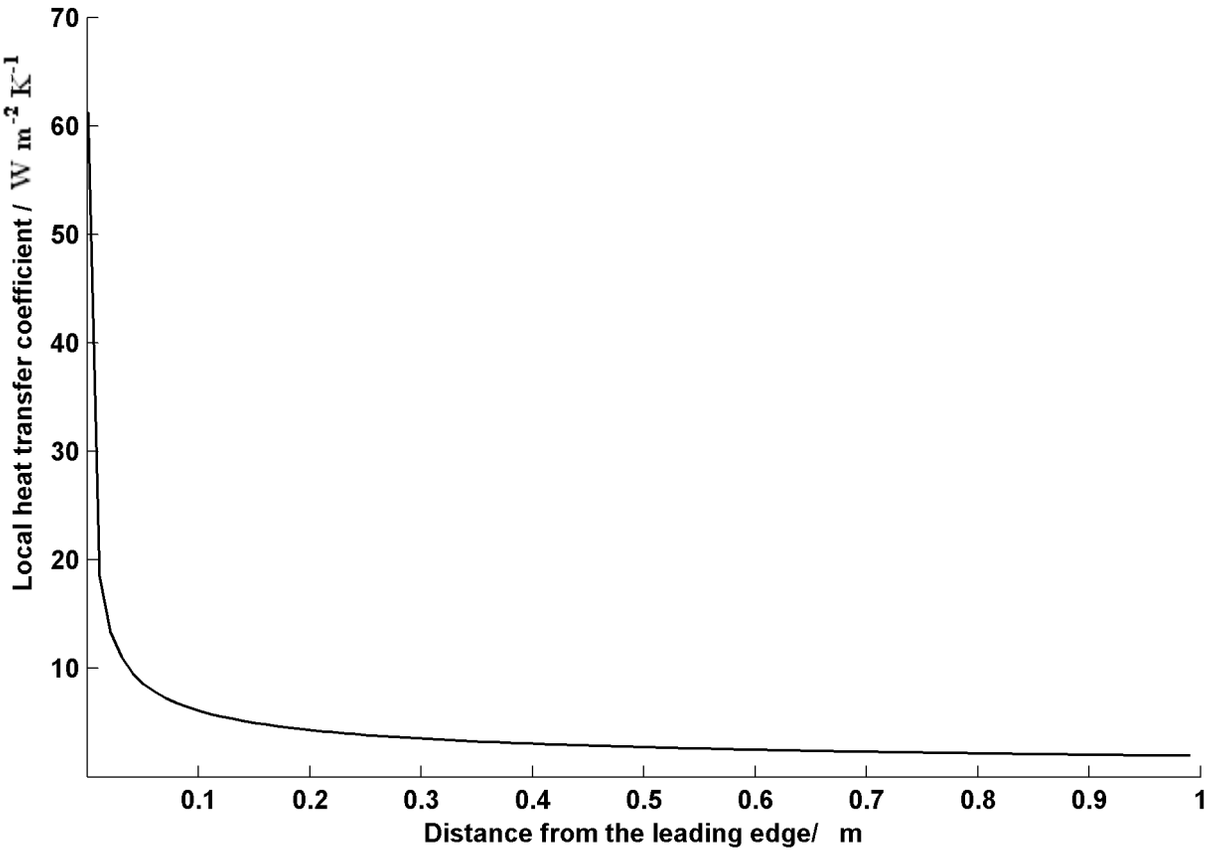

Figure 8. Local heat transfer coefficient vs. distance from the leading edge.

A model proposed in a previous paper [26] was modified to find a method for prediction of surface temperature distribution. The equation of energy can be represented as:

$$\varrho\ cp\ \frac{\partial T}{\partial t} = \nabla(k\nabla T) + \nabla(\frac{D_v M}{RT}\nabla P_v)\Delta hv \tag{2}$$

At time zero, the whole body has a uniform initial temperature of T_o, and the initial conditions are:

$$T_o = T\big|_{y=0} = T\big|_{y=h} \tag{3}$$

At the external surface, i.e. y=0, the boundary conditions can be written on the basis of Figure 9 as:

$$-k\ \frac{\partial T}{\partial y} = h\,(T_a - T_{sx}) + \dot{m}\ \Delta hv \tag{4}$$

where T_{sx} is the surface temperature at distance x from the leading edge.

The drying rate, $\dot{m}$ varies with the time and can be defined as,

$$\dot{m} = \frac{M\,K'_G}{RT}\left(P_{sr} - P_v\right) \tag{5}$$

where K'_G is an overall mass transfer coefficient, defined in [27] as:

$$\frac{1}{K'_G} = \frac{1}{k'_c} + \frac{z''}{D_{eff}} \tag{6}$$

where k'_c is the local mass transfer coefficient (m s^{-1}), z" is the distance from the plate surface to the receding evaporation front in (m).

The boundary condition at y = h is:

$$-k\ \frac{\partial T}{\partial y} = 0 \tag{7}$$

Equation (2), with such boundary conditions, was solved by a finite difference method (a modified form the so-called explicit method). Therefore, the temperature distribution on the surface (i.e. y = 0) was calculated by using the model at different local points, x. Table 1 shows the physical properties of the sample materials.

http://dx.doi.org/10.5772/54322

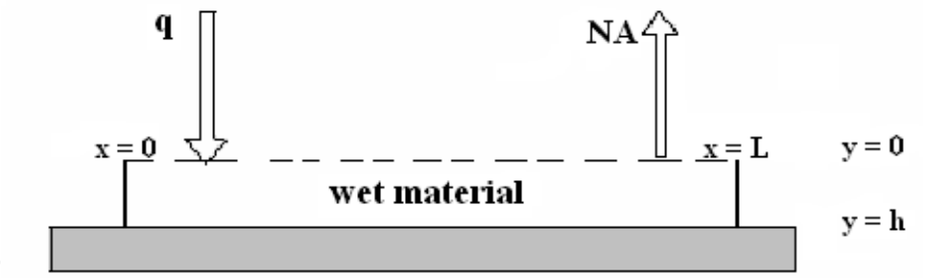

Figure 9. Heat and mass transfer process for the wet material. NA: mass transfer flux and q: heat transfer flux.)

Figure 10 shows the experimental and the predicted surface temperature distributions for the desert sand along the bed at various times. The predicted temperatures were in good agreement with the experimental results. From the graph, it can be seen that there is a significant difference in the surface temperature between 0.1 m and 1 m. At time=195 minutes; i.e. during the constant-rate period, the difference in temperature was 2 °C.

During the falling-rate period, the difference in the surface temperature between 0.1 m and 1 m increased. At 510 minutes, the difference is 11 °C. At the bottom of the sand bed, the difference in temperature along the bed also can be seen clearly (Figure 4).

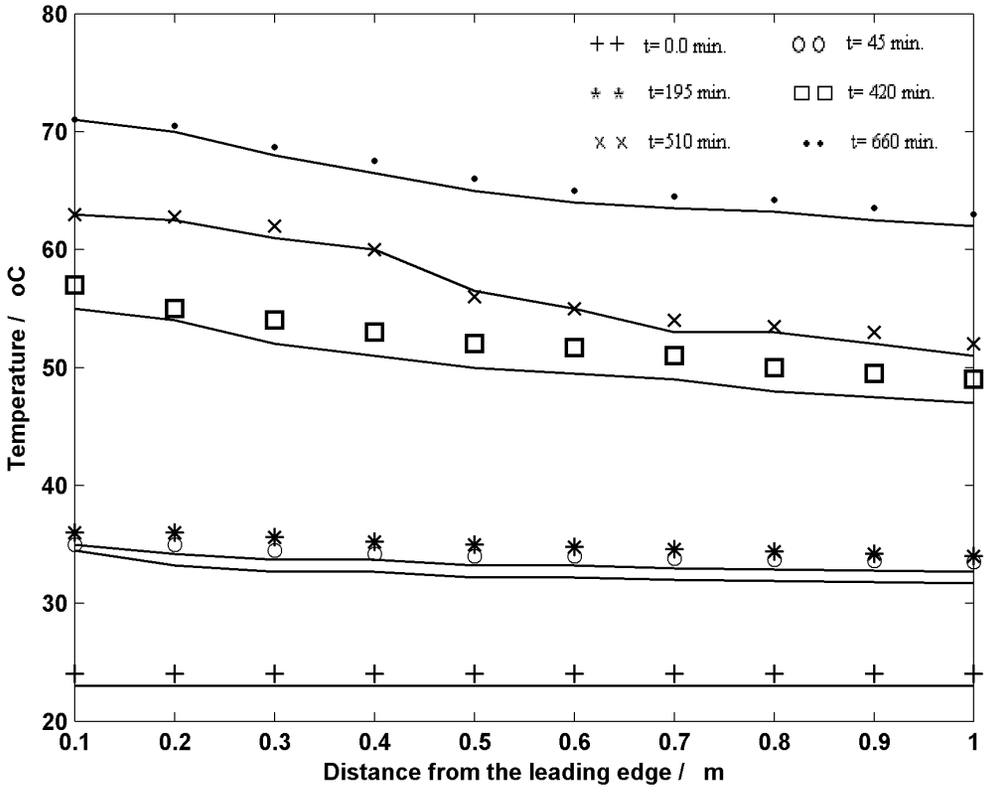

Figure 10. Experimental and predicted surface temperatures of the desert sand bed; experimental results (symbols); predicted results (solid lines).

For the entire time of the experiment, the surface and the bottom temperatures decreased gradually with increasing distance from the leading edge. This caused by the resistance to heat transfer process which increased with increasing thickness of thermal boundary layer. In contrast, near the leading edge, the resistance to heat transfer diminishes, since the thickness of the thermal boundary layer in the vicinity of the surface thins. Therefore, the rate of heat transfer to the body increased, thereby raising the temperature of surface. Afterwards, heat transfer by conduction across the solid particles raises the temperature of the bed, and the portion closest to the leading edge dries faster than that at a greater distance.

Figure 11 shows both predicted and experimental results for the bed of beach sand. This Figure shows that the computed temperature distribution was in general agreement with experimental results. However, unsatisfactory results can be seen at times greater than 400 minutes, i.e. during the falling-rate period. This is due to the nature of the beach sand as discussed before. The surface temperature of the beach sand sample decreased gradually with increasing distance from the leading edge. A significant difference in temperature between 0.1 m and 1 m can be seen clearly for both constant and falling-rate periods. During the constant-rate period, the difference in temperature was 2 ^{o}C, whereas in the falling-rate period the difference reached to 8 ^{o}C.

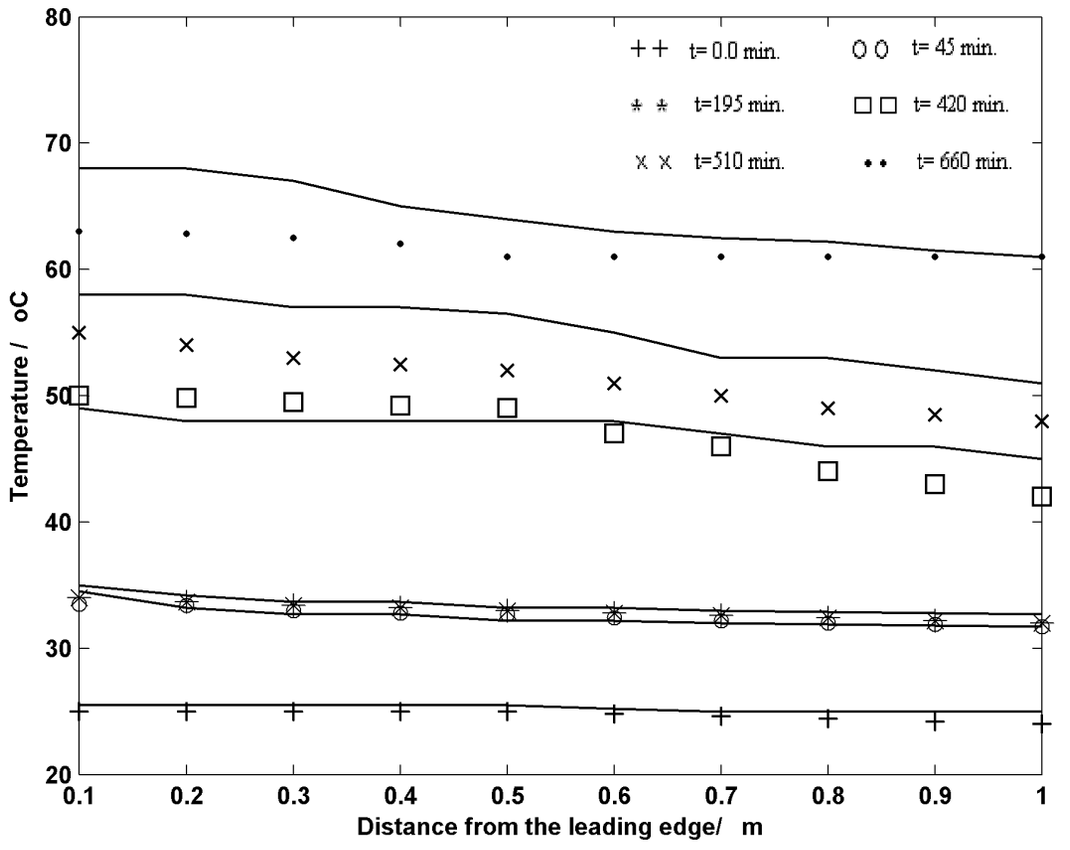

Figure 11. Experimental and predicted surface temperatures of the beach sand bed; experimental results (symbols); predicted results (solid lines).

http://dx.doi.org/10.5772/54322

	ρ(Kg/m^3)	cp_d (kJ/kg K)	k (W/m K)	k_d (W/m K)	D_{eff} (m^2/s)	D_v (m^2/s)
Desert sand	1760	1.1	0.760	0.246	0.81×10^{-5}	1.75×10^{-5}
Beach sand	1980	1.2	1.12	0.188	1.15×10^{-5}	2.05×10^{-5}

Table 1. Physical properties for desert sand and beach sand.

We have found that the temperature distribution profiles determined for the flat beds of desert sand, beach sand and glass beads identified clearly the stages of drying. The temperature profiles in general were almost similar. However, the beach sand profile showed irregularity in temperature, due to the nature of the beach sand which contains a lot of shells with various shapes.

The temperature profiles also showed that when the whole surface of the bed became dry, the whole bottom of the bed remained wet. During the falling-rate periods, a receding evaporation front divided the system into a hotter, dry zone near the surface and a wet zone towards the bottom of the sample.

The predicted transport coefficients have very large values close to the leading edge, where the thickness of the boundary layer approaches zero. In contrast, the values of the coefficients decrease progressively with increased distance from the leading edge, where the boundary layer thickens. Hence the resistance to heat and mass transfer to, or from, the surface also increases. These variations in thickness and resistance have a significant effect on the temperature distribution along the bed and the drying rate.

A mathematical model has been modified to predict temperature distributions along the bed at various times. The model was compared with the experimental results for various beds and good agreement was obtained. We found that surface and bottom temperatures decreased gradually with increasing distance from the leading edge, and the difference in temperature became clearer during the falling-rate period. The difference in the surface temperature was 11 ^{o}C for the case of desert sand, and was 8 ^{o}C for the case of beach sand. We concluded that the portion close to the leading edge dried faster than that at larger distance, since the resistance to heat and mass transfer diminishes at that position.

3. Single droplet drying

The study of mechanisms that describe single droplet drying is a challenging issue since it involves many disciplines: heat and mass transfer, fluid mechanics and chemical kinetics. The main objective of this section is to attempt to further understand the mechanisms involved in the drying of a single droplet, and more specifically to formulate a mathematical model. The model should predict temperature profiles for both the inner core and the outer surface of the droplet under simulated conditions that might be encountered in spray drying equipment. Experimental work will also involve the measuring the moisture contents against time to provide more information for the droplet drying process.

The experimental apparatus was comprised of a horizontal wind tunnel 2.2 m long. The wind tunnel supplied a forced drying air into the working section where the droplet was suspended from a glass nozzle. The apparatus and the flow system are shown in Figure 12. A gate valve at the inlet to the wind tunnel controlled airflow rate. Air was heated to the desired temperature, using a 3 KW electric heating element controlled by a rotary voltage regulator.

Through the wind tunnel, a controlled flow of hot, dry air, with an average velocity of 1 m/s, was passed across the droplet suspended from the glass nozzle. A forced dry air was obtained by using a centrifugal fan and a molecular sieve air dryer containing silica gel and calcium silicate.

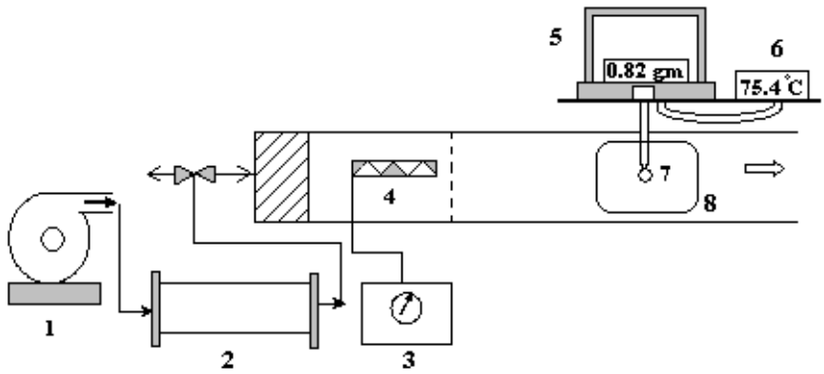

Figure 12. Experimental apparatus: 1-fan 2-molecular sieve 3-voltage regulator 4-air heater 5-Digital balance 6-Temperature recorder 7-Glass nozzle 8-Observation port.

The experiment was initiated by switching on the centrifugal fan and then the electric air heater. The voltage regulator was adjusted to provide the desired air temperature. A thermocouple was fixed in the wind tunnel near to the glass nozzle to measure the air temperature with an accuracy of ± 1° C. The air temperature was monitored until it reached a steady state. This state requires between 1 to 2 hours to be achieved. When the apparatus achieved a constant air temperature, the drying process was initiated.

As a part of this study, a droplet suspension device was specially designed to measure the weight and temperature of the droplet. The droplet suspension device is illustrated in Figure 13. It consisted of a glass nozzle with the dimensions of 180 mm in length and 9 mm outside diameter. The upper section of the glass nozzle was fixed by a small electric rotator device able to provide a rotational speed range of 1- 30 rpm. In order to reduce the contact area between the free end of the glass nozzle and the droplet surface, the lower section of the nozzle was shaped as a small cone with a free end diameter of 4 mm. The droplet receives a relatively small amount of heat transferred by conduction through the glass nozzle, which has a thermal conductivity of 0.480 W/m K. The heat transferred by conduction was taken into account in the proposed model represented by Equations 4&5. The glass nozzle was rotated at constant low speed of 5 rpm. This rotation speed had no effect on the shape or stability of the droplet. The upper section of the suspension device was fixed by a metallic

http://dx.doi.org/10.5772/54322

clip installed beneath the analytical balance. The lower section of the suspension device, i.e. the glass nozzle, was inserted through a hole in the wind tunnel.

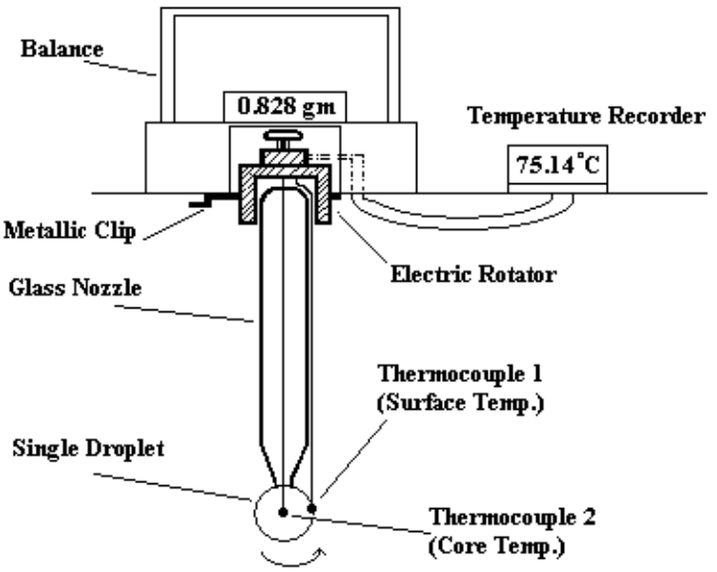

Figure 13. Droplet suspension device; glass nozzle and the connected thermocouples.

Two thermocouple sensor types, NiCr-NiAl, were used to measure the core and surface temperatures of the droplet. One of the thermocouples was placed inside the glass nozzle and extended to the center of the droplet. The other thermocouple was fixed outside and along the glass nozzle. The outer thermocouple rotates simultaneously with the rotation of the glass nozzle. The end tip of the thermocouple was positioned in a manner to touch the outer surface of the droplet. The rotation process that made both the nozzle and the droplet rotate together assisted in avoiding any separation between them that might have been caused by the force of air drying. The core and the surface temperatures of the droplet were easily recorded by a temperature recorder at 50 sec. intervals. The drying process of the different material droplets was investigated under air temperature of 75° C and 140° C.

The procedure for weighing the droplet was carried out quickly and intermittently by causing the suspension device to be freely-suspended. The gate valve was closed to cut off the airflow to the working section and diverted to an outlet 20 mm valve in order to prevent any vibration of the glass nozzle during the weighing process. The nozzle rotation was simultaneously stopped. A metallic clip was opened manually to allow the suspension device to be freely-suspended from a hook connected beneath the balance. This arrangement made the weight measurement readings more accurate. The weighing procedure was repeated during the droplet drying experiment at 100 secintervals. Thus, the weight loss of droplet was recorded and moisture content was determined versus time. The required time for each weighing procedure step was about 10 sec. This time was not included in the recorded drying time and had no noticeable effect on the results.

Three types of liquids were selected for the drying process experiments. The first type was sodium sulphate decahydrate solution (60 wt % solid). The second type was a concentrated fruit juice (60 wt % fruit juice powder of apple, peach and blueberry, MTC product). The third type was an organic paste (20% sodium chloride, 25% dispersal pigment; Goteks product) used for adhesive and coating applications. Table 2 shows the physical properties of the sample materials. Droplets ranging from 9 mm to 14 mm diameter were subjected to the drying process. However, the actual size of the droplets in typical spray drying applications is much smaller. The droplets with small sizes require developing a more accurate technique to measure both core and surface temperatures. Therefore, the current research assumes that the mechanisms of the drying large and small droplets are similar.

	ρ_d (Kg/m^3)	cp_d (kJ/kgK)	k (W/mK)	k_d (W/mK)	D_{eff} (m^2/s)	D_v(m^2/s)
Sodium sulphate decahydrate solution	3110	1.1	0.180	0.246	1.14x10^{-5}	3.45x10^{-5}
Fruit juice	1650	1.7	0.126	0.188	1.10x10^{-5}	3.40x10^{-5}
Organic paste	3400	2.4	0.251	0.422	1.52x10^{-5}	3.50x10^{-5}

Table 2. Physical properties of sodium sulphate decahydrate solution, fruit juice and organic paste.

3.1. Mathematical model

In the drying process, the droplet is first heated by the hot air flow with significant evaporation from the surface. The temperature of the surface increases and approaches the wet-bulb temperature, indicating the constant drying rate period. In order to propose a mathematical model, the droplet was assumed to have a fixed size with no change during this period. Also, the droplet was assumed to have a uniform initial temperature and moisture content. Temperature distribution within the droplet can be represented as

$$\frac{\partial T}{\partial t} = \alpha\left(\frac{\partial^2 T}{\partial r^2} + \frac{2}{r}\frac{\partial T}{\partial r}\right) \tag{8}$$

Equation 8 was solved with the following boundary conditions using explicit finite differences,

$$-k\frac{\partial T}{\partial r} = 0 \qquad at\ r = 0 \tag{9}$$

and

$$-k\frac{\partial T}{\partial r} = h(T_a - T_{sr}) + q_{nz} \qquad at\ r = R \tag{10}$$

http://dx.doi.org/10.5772/54322

where, q_{nz} is the transferred heat conduction to the droplet through the glass nozzle. It can be calculated as:

$$q_{nz} = \left(\frac{4 k_{nz} h_{nz}}{d_{nz}}\right)^{0.5} (T_a - T_{sr}) \tag{11}$$

The heat transfer coefficient, h_{nz}, can be correlated from Thomas (1999) as:

$$h_{nz} = 0.26 + Re^{0.6} Pr^{0.33} \left(k_{air} / d_{nz}\right) \tag{12}$$

During the falling rate period, the formation of a receding evaporation front divides the droplet into two regions, a dry crust at the outer surface and a wet region inside the core. Therefore, heat transfer equations are formulated for each region. The physical model and the coordinate system for analysis are shown in Figure 14.

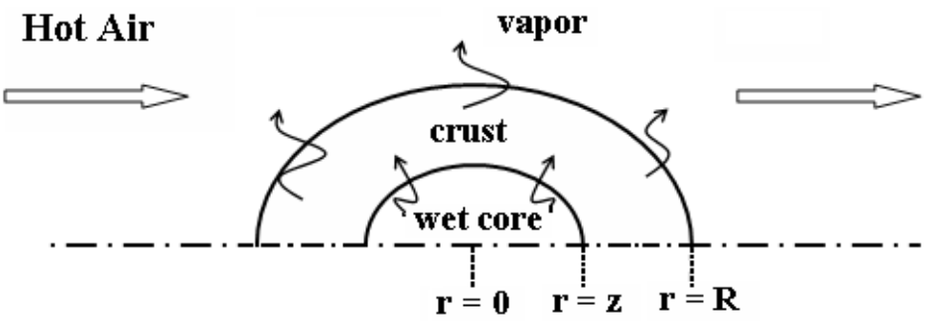

Figure 14. Physical model and the coordinate system of the droplet cross-section.

Energy balance for the wet core, $0 < r < z$, can be represented as follows:

$$\frac{\partial T_w}{\partial t} = \alpha_w \left(\frac{\partial^2 T_w}{\partial r^2} + \frac{2}{r}\frac{\partial T_w}{\partial r}\right) \tag{13}$$

Heat is transferred through the crust into the wet core where evaporation occurs at the interface between the core and the crust. Vapor then diffuses through pores of the crust into the drying medium. Thus, moisture is transferred mainly by vapor flow. Consequently, vapor diffusion must be taken into account in formulating the equations for the dry (crust) region. The energy balance for the crust region, $z < r < R$, can be represented as follows:

$$\frac{\partial T_d}{\partial t} = \alpha_d \left(\frac{\partial^2 T_d}{\partial r^2} + \frac{2}{r}\frac{\partial T_d}{\partial r}\right) + \frac{\partial}{\partial r}\left(\frac{M}{RT}\frac{\partial P_v}{\partial r}\right)\frac{\Delta h_v}{\rho_d c p_d} D_v \tag{14}$$

3.2. Boundary conditions

At the center of the sphere, r = 0

$$-k_w \frac{\partial T_w}{\partial r} = 0 \tag{15}$$

At the surface, r = R:

$$-k_d \frac{\partial T_d}{\partial r} = h(T_a - T_{sr}) + q_{nz} \tag{16}$$

At the receding evaporation front (r = z), the moving boundary conditions are

$$-k_d \frac{\partial T_d}{\partial r} + k_w \frac{\partial T_w}{\partial r} = \dot{m}\, \Delta hv \tag{17}$$

The drying rate, $\dot{m}$, was defined in Eqs. (5 & 6). However, in this case, z'', in Eq. (6) represents the distance from the droplet surface (r = R) to the receding evaporation front (r = z).

Heat and mass transfer coefficients, h and k_c', can be determined by the correlations found in [28,29] as follows:

$$Nu = 2 + \Phi Re^{0.5} Pr^{0.33} \tag{18}$$

and

$$Sh = 2 + \beta Re^{0.5} Sc^{0.33} \tag{19}$$

where Φ and β are constants ranging from 0.6-0.7 for Re (500 -17000).

Thermal conductivity of the wet region can be evaluated according to [30] as:

$$k_w = k_d + k_v \overline{X} \tag{20}$$

where $\overline{X}$ is an average moisture content and k_v is

$$k_v = \frac{D_v M}{RT} \cdot \frac{dp}{dT} \Delta h_v \tag{21}$$

http://dx.doi.org/10.5772/54322

The non-linear Eqs. (13&14) with the boundary conditions as in Eqs. (15-17) were solved by a finite difference method. The proposed equations were solved in a program using Turbo-Pascal V.6, and the computational results compared with the experimental results.

3.3. Results

A single droplet of sodium sulphate decahydrate solution was suspended from the free end of the glass nozzle at an air temperature of 75° C and an air velocity of 1 m/s. The wet-bulb temperature was 46° C. The core and surface temperatures of the droplet versus time are plotted in Figure 15. Initially, the temperatures increased rapidly because of the large difference in temperature between the drying medium and the droplet. Basically, the plot exhibited two drying periods. A short period, from time =100 - 200 s, where the surface temperature approached the wet-bulb temperature, is described as the constant rate period. The second period, or falling rate period, extended from t =200 s to the end of the experiment.

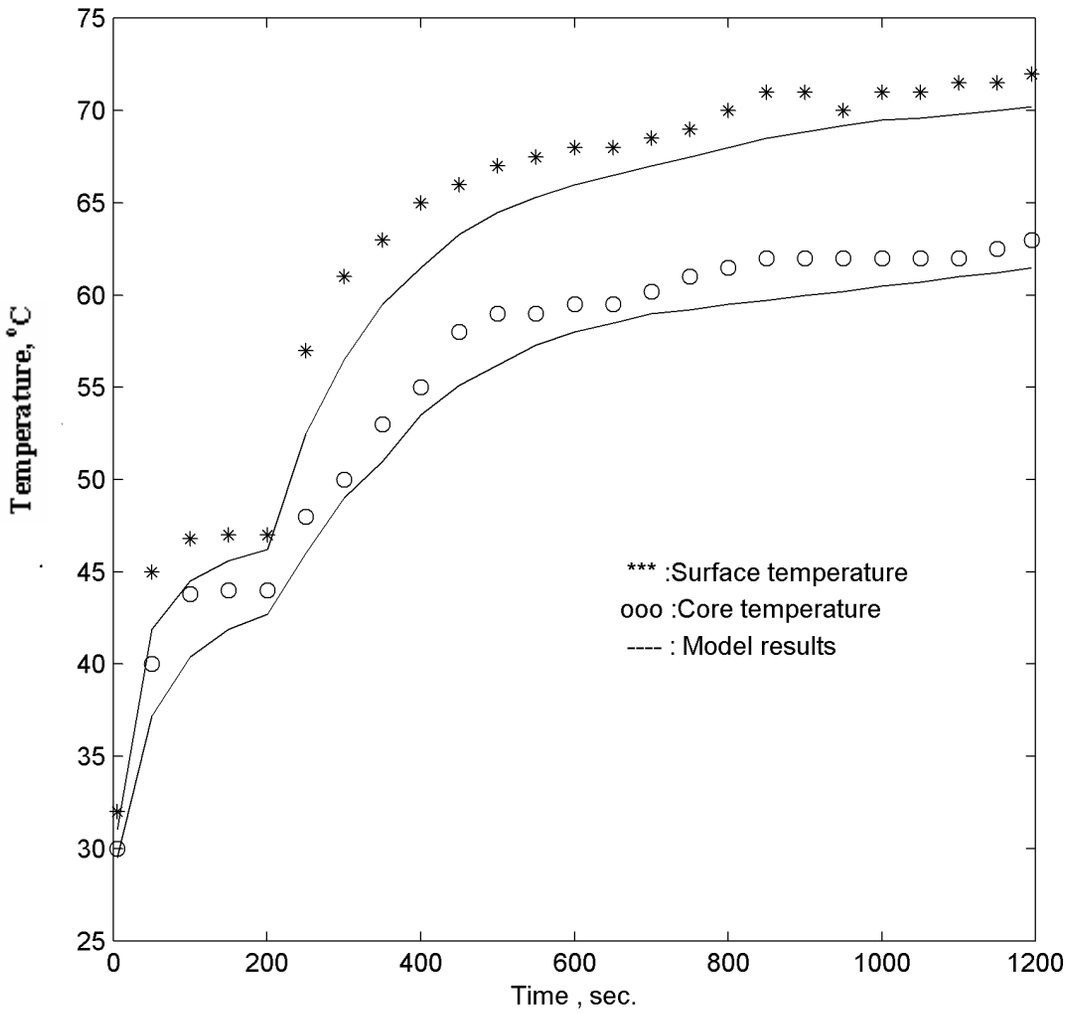

Figure 15. Temperature distribution profile for sodium sulphate decahydrate at air temperature of 75° C.

Figure 15 plots the predicted values of both the core and surface temperature evaluated by the developed model. Comparison of the experimental and theoretical results showed good agreement. However, actual surface temperatures were slightly higher than those predicted by the model. This probably was due to the position of the thermocouple and its reading during the experiment, as will be discussed later in more detail.

The previous experiment was repeated at an air temperature of 140° C in the same drying medium. Figure 16 shows experimental and theoretical results of a droplet of the same material. The experimental results showed that the constant rate period extended from time= 85 - 165 s, shorter than that observed at 75° C. The results showed both surface and core temperatures of 130° C at 900 s, at which point the droplet had dried completely. Figure 16 showed agreement between the experimental and predicted results.

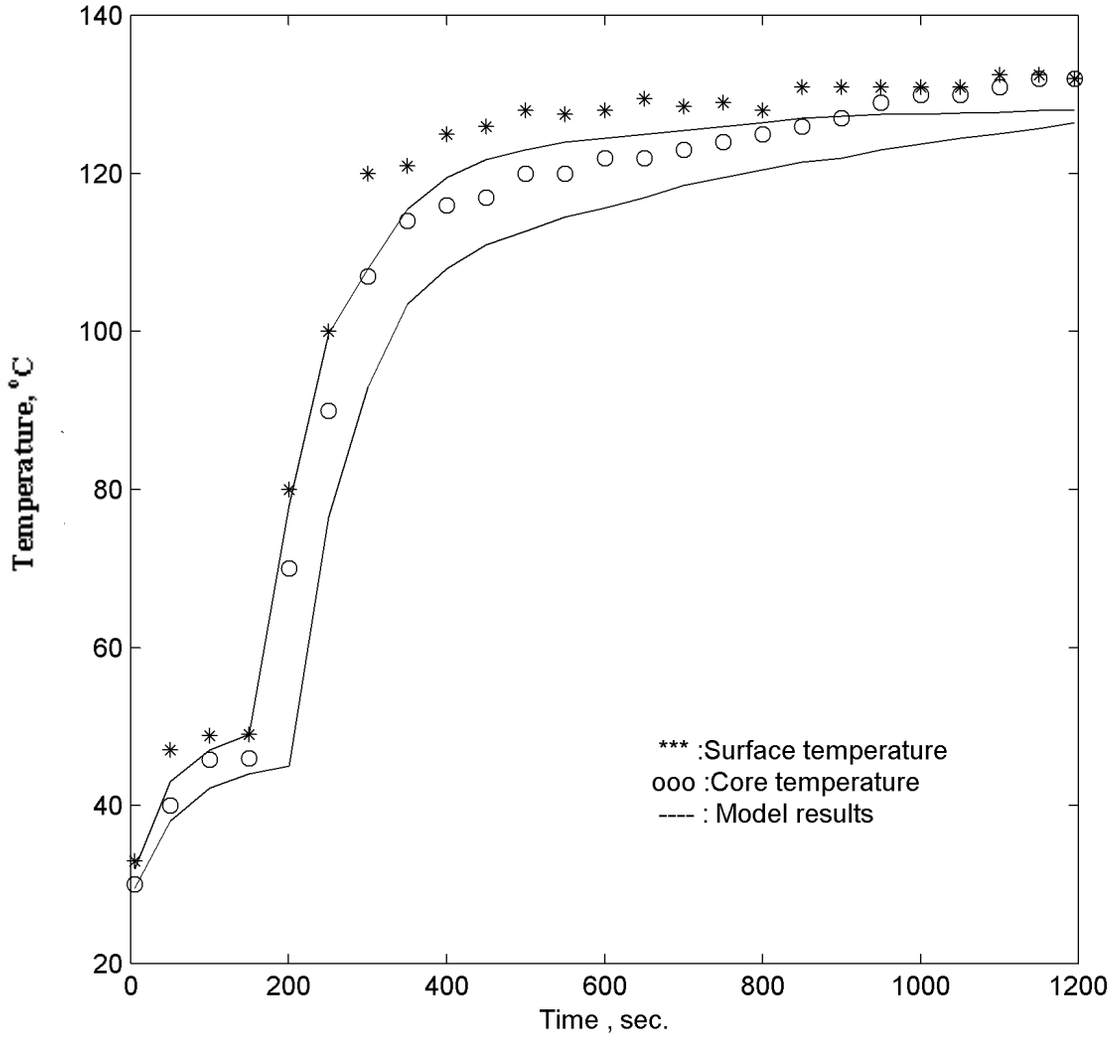

Figure 16. Temperature distribution profile for sodium sulphate decahydrate at air temperature of 140° C.

A single droplet of a fruit juice was dried at an air temperature of 75° C and an air velocity of 1 m/s. Wet-bulb temperature was 44.5° C. The experimental results in Figure 17 show a con-

http://dx.doi.org/10.5772/54322

stant rate period from time =100 - 200 s. The falling rate period can be observed after the constant period, when the temperature increased quickly.

During the falling rate period some experimental readings represented approximate values of the actual droplet surface temperatures. The approximate values can be attributed to the fact that the droplet diameter constantly decreased with time and that caused the distance between the tip of thermocouple and the surface of droplet to grow. In other words, during some time in the experiment, a part of the end tip of the thermocouple was touching the surface of the droplet, and the remaining area of the tip was exposed to air flow. Such a behavior caused the tip of thermocouple to give an average reading for both the surface and the air flow temperatures. Good agreement was obtained between the theoretical and experimental results of the temperature profile for the fruit juice.

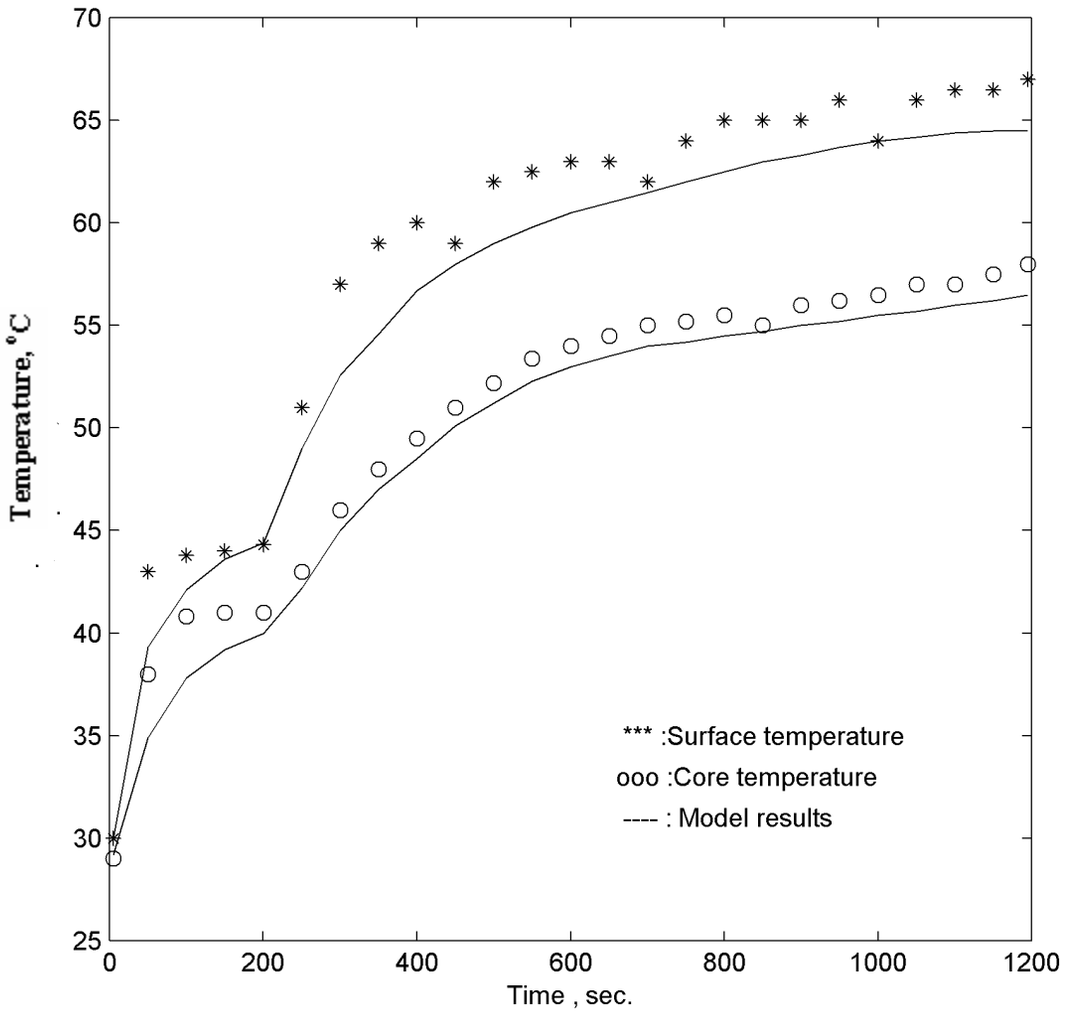

Figure 17. Temperature distribution profile for fruit juice at air temperature of 75° C.

The fruit juice droplet was dried again at an air temperature of 140° C in the same drying medium. The results (Figure 18) showed that the constant rate period was a little shorter

than that at 75° C. The results showed also that both surface and core temperatures were similar and close to the air temperature at time = 1050 s. The mathematical model showed also good agreement with the experimental readings.

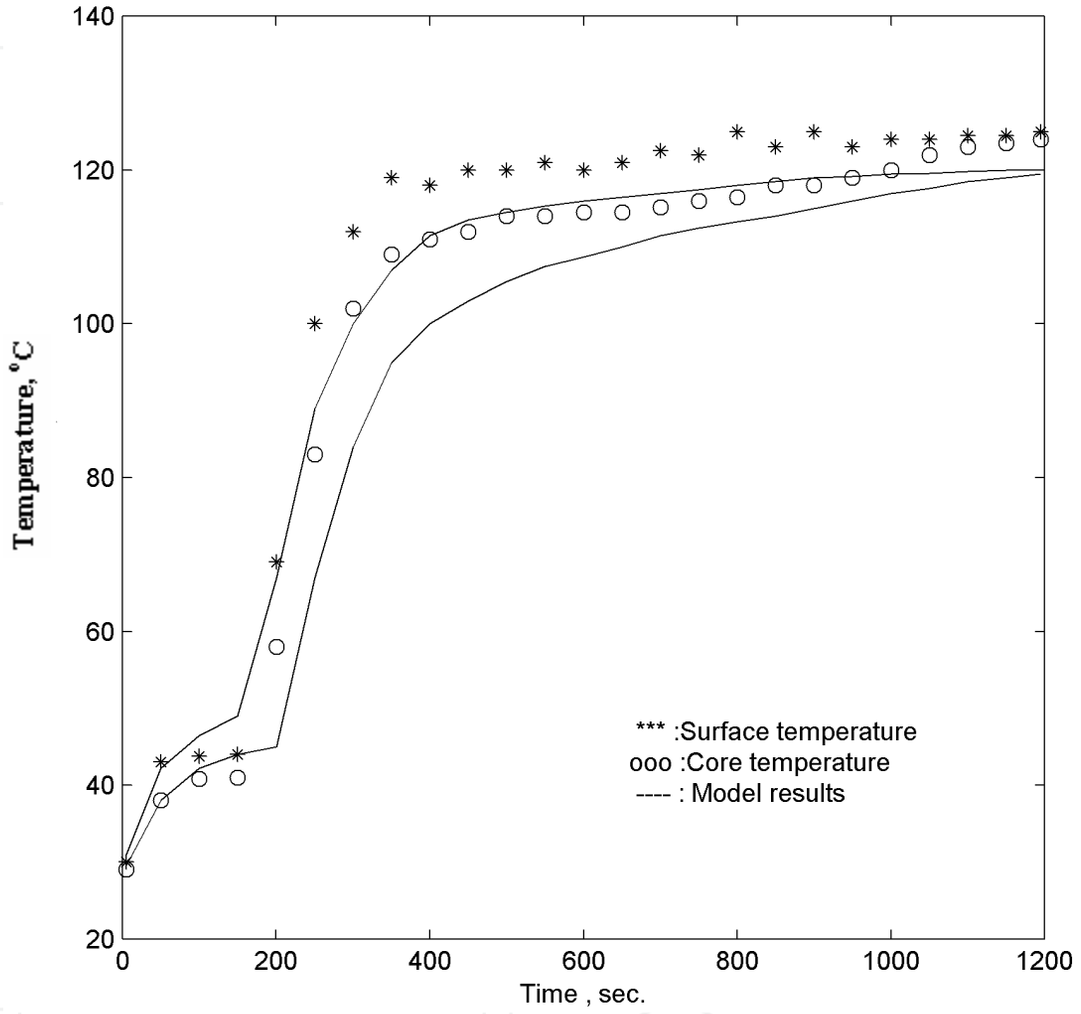

Figure 18. Temperature distribution profile for fruit juice at air temperature of 140° C.

A single droplet of organic paste was dried under similar conditions to that of the fruit juice. A plot of the core and surface temperatures of the droplet versus time is shown in Figure 19. A relatively longer period of constant drying rate, compared to those shown for sodium sulphate and fruit juice, was observed. Figure 19 also showed that surface temperature increased rapidly after time = 300 s, indicating the beginning of the falling rate period. Less agreement was obtained between the model's predicted results and the experimental results. Organic paste, which has higher thermal conductivity, forms a thicker solid crust at the outer surface compared to the other material evaluated. Therefore, a higher resistance to heat and vapor through the crust would be expected. To improve the predictions, introduction of a correction factor is probably required in the model for those materials which have a nature similar to that of the organic paste. Figure 20 shows the experimental and theoretical

http://dx.doi.org/10.5772/54322

results of air temperature of 140° C. Again, forming a solid crust at the outer surface led to less agreement between theoretical and experimental results. The predicted temperature distributions were higher than the actual temperatures.

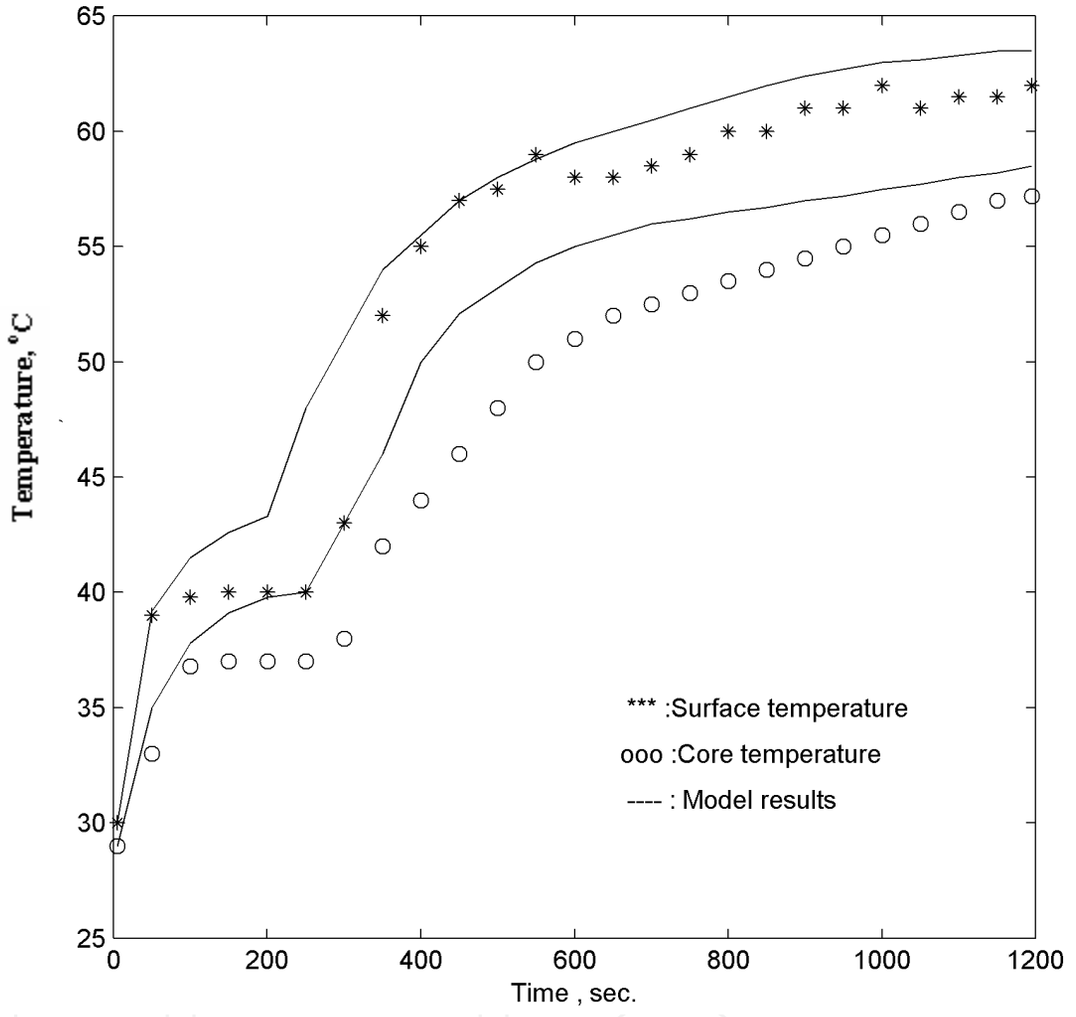

Figure 19. Temperature distribution profile for organic paste at air temperature of 75° C.

The moisture content of the droplet was determined by measuring the weight loss against time. There was no experimental technique to measure core and surface moisture content separately; therefore, the measured moisture content of the droplet represented the average value. The experimental results of moisture content distribution for the three samples at an air temperature of 75° C, are shown in Figure 21. The moisture content profiles clearly show the two stages of drying, the constant rate period and the falling rate period. The profiles show that the sodium sulphate decarbohydrate solution had consistently lower moisture content, as it dried faster than the other materials. The profiles also showed that forming a solid crust in the falling rate period lowered the moisture content values for all the three samples. In the case of organic paste, the change in the moisture content was more significant.

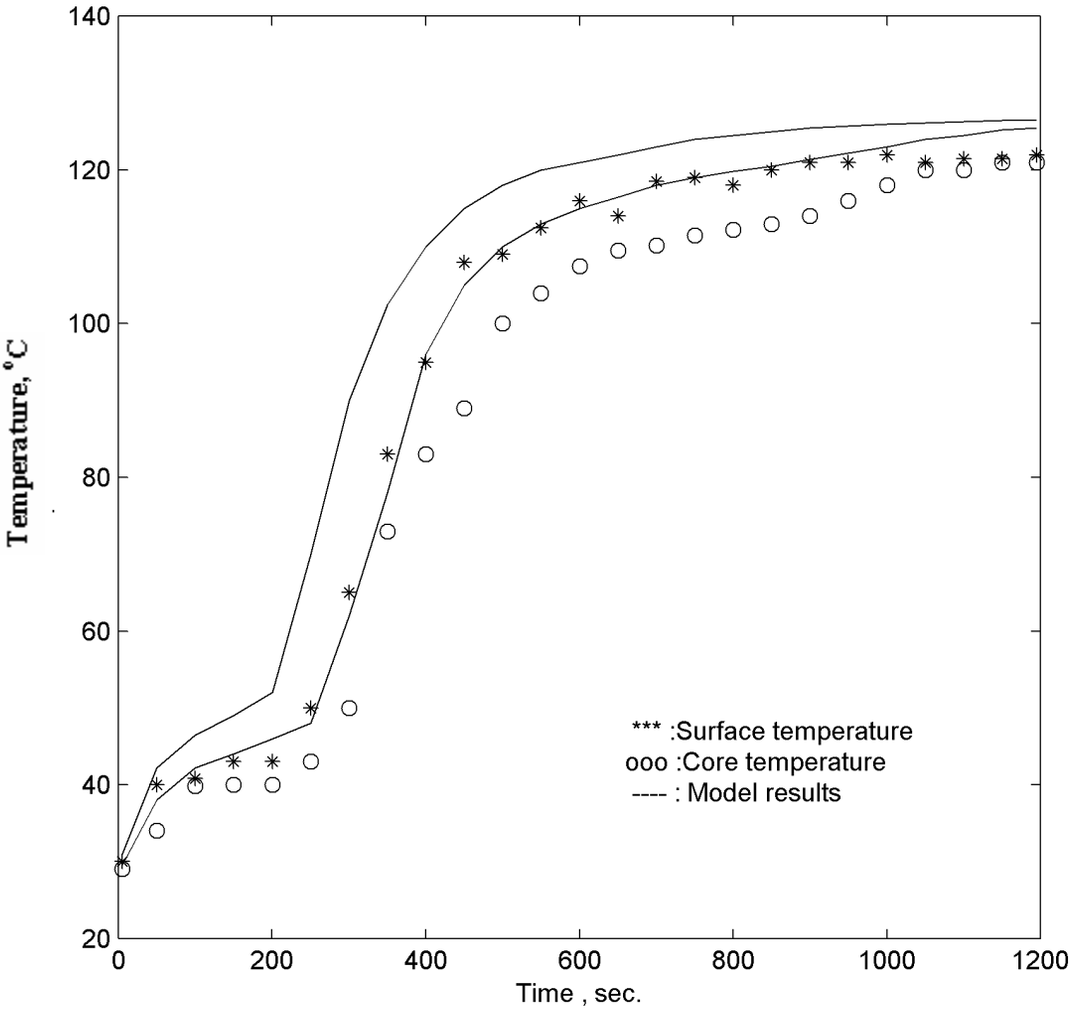

Figure 20. Temperature distribution profile for organic paste at air temperature of 140° C.

Obviously, crust formation, thickness and porosity have a significant effect on the moisture content and on the drying rate of the droplet. This result was also obtained by Hayder & Mumford [31] in the drying of custard and starch droplets. They observed that crust formation was more rapid on the custard droplet, because the smaller starch granules absorbed less and left more free water in the droplet. Therefore, the crust growth and the drying rate of the starch droplets took a longer time.

Moisture distribution curves for the three samples at 140° C air temperature are plotted in Figure 22. Similar results were obtained to those observed at an air temperature of 75° C. Also, the profiles showed that the moisture content dropped to lower values compared to those at 75° C. In other words, the droplets dried faster at the higher temperature.

3.4. Discussion

As previously observed, moisture and temperature distribution profiles of various materials exhibited constant and falling drying rate periods. In the constant rate period, the tempera-

http://dx.doi.org/10.5772/54322

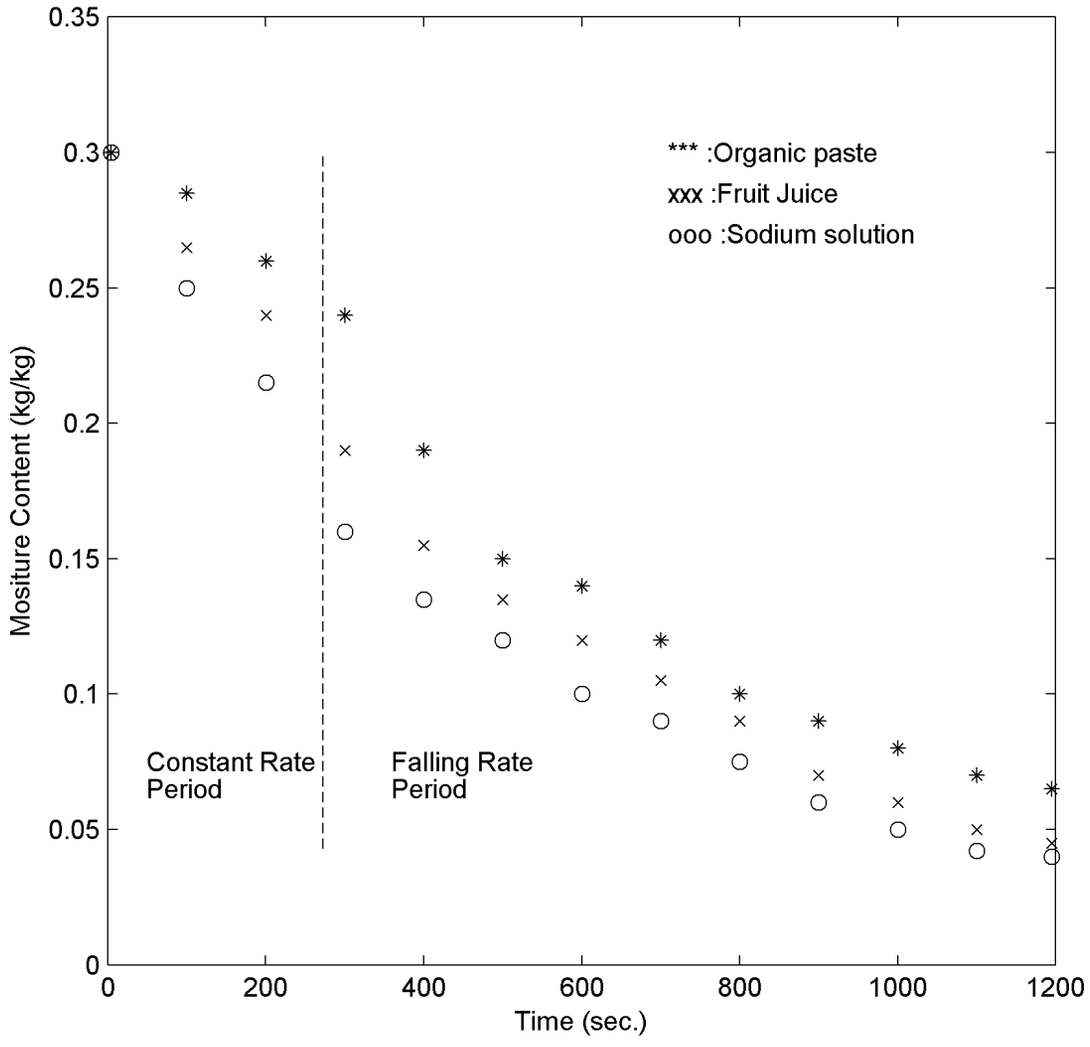

Figure 21. Moisture content profile for all samples at air temperature of 75° C.

ture of the droplet surface was almost equal to the wet-bulb temperature. During this period, evaporation takes place from the free liquid surface of the droplet. The constant rate period was relatively short in sodium sulphate and fruit juice samples. However, that period was longer in the case of organic paste.

The falling rate period is characterized by formation of a partial crust on the outer surface of the droplet. This crust recedes towards the core and the surface temperature starts to increase. Vapor diffusion becomes the predominant transport process at this stage. Crust structure, thickness and porosity have a significant effect on the rate of drying. The crust thickness increases with time, hence the resistance to heat and moisture diffusion through the crust increases. Therefore, moisture content and drying rate decrease.

Some experimental readings represented approximate values of the actual droplet surface temperatures. This was attributed to the end tip of thermocouple that was giving average readings for both the surface and the air flow temperatures at the same time. It was also as-

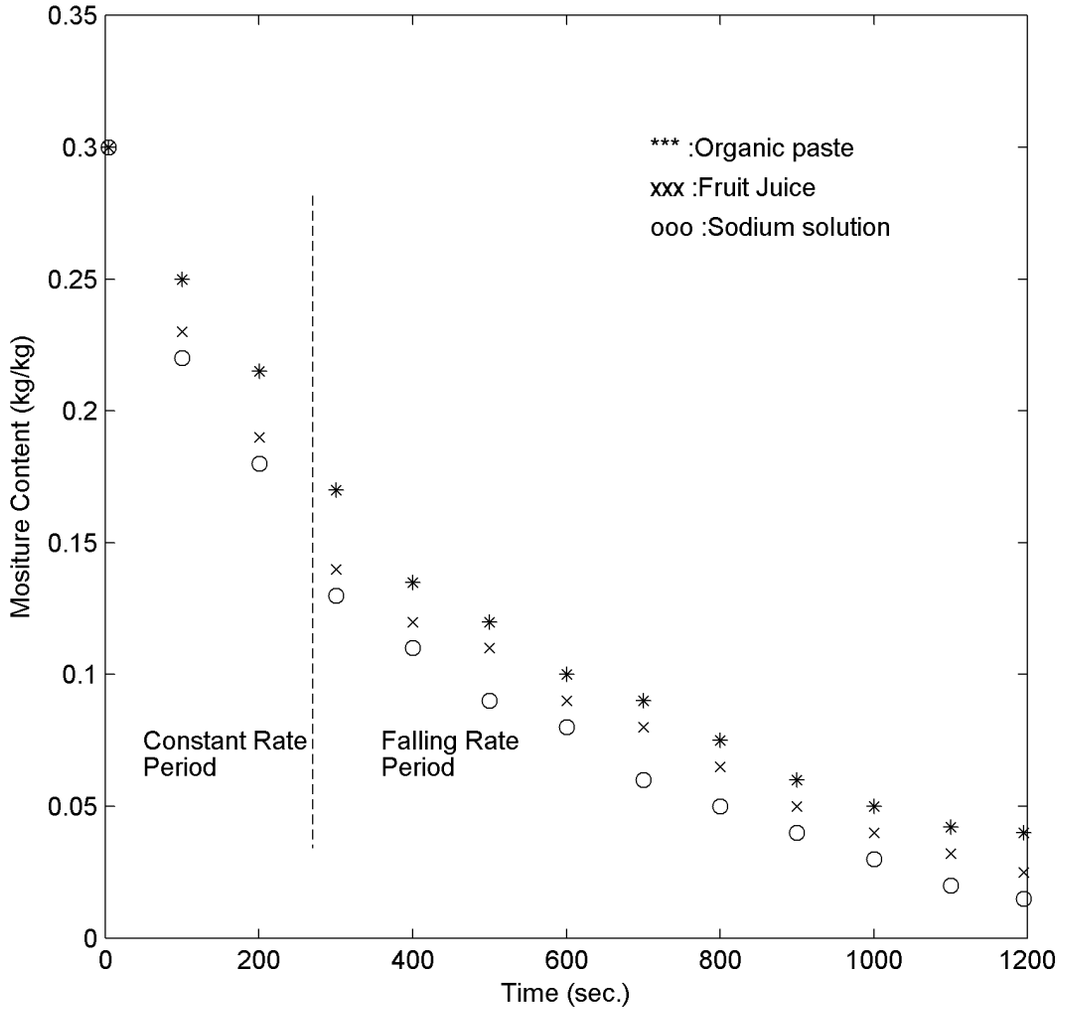

Figure 22. Moisture content profile for all samples at air temperature of 140° C.

sumed that the mechanism of the droplet drying is similar for both small and large diameters. Therefore, it is recommended that a more accurate technique for measuring droplets with small sizes and for the taking of surface temperatures be developed.

The new model predicted temperature distribution profiles for single droplets of various materials. The predicted results showed a good agreement with the experimental data for air temperatures at 75° C and 140° C. However, the model was less accurate in the case of organic paste due to the higher thermal conductivity of the formed crust. A correction factor should be developed and taken into account for such materials. The model provides a relatively fast and efficient way to simulate drying behavior over a range of drying conditions. The model also represents a useful tool in the design and optimization of spray drying processes.

Moisture content profiles clearly showed the two stages of the drying process. In addition, the moisture profiles supported the conclusions that the crust forming in the falling rate period decreased both the moisture content and the drying rate.

http://dx.doi.org/10.5772/54322

Through the results of the experimental work and the theoretical model for a droplet drying, a significant conclusion was obtained. It has always been wrongly assumed in the literature that there is no temperature distribution within the droplet. This concept has been corrected by the current research. All experiments for the three materials used showed a clear difference between the core and the surface temperatures of the droplet during the drying process.

3.5. General conclusion

The characteristics of the boundary layer have a great effect on the local heat and mass transfer coefficients and temperature distributions throughout a flat bed surface. Droplet drying is an important subject in drying science, since it provides more details about the drying mechanisms in order to optimize spray dryer equipment. However, this part of the drying field is rarely considered in the literature. Further research in this area seems essential to obtain better understanding of drying theory.

Wind tunnel definitely is considered one of the best tools to investigate and to study the mechanisms of drying process. The most important variables in any drying process such as air flow, temperature and humidity are usually easy to be controlled inside the wind tunnel. Through a mathematical approach and an experimental work using a wind tunnel, we highlighted on the role of the boundary layer on the interface behavior and the drying mechanisms for various materials of a flat plate surface and a single droplet shape.

Nomenclature

α	Thermal diffusivity	m^2/hr
Cp	Heat capacity	kJ/kg K
D	Diameter	M
D_{eff}	Effective diffusivity	m^2/s
D_v	Diffusivity of vaporization	m^2/s
H	Heat transfer coefficient	W/m^2 K
Δh_v	Latent heat of vaporization	kJ/kg
K	Thermal conductivity	W/m K
k'_c	Mass transfer coefficient	m/s
K'_G	Overall mass transfer coefficient	m/s
M	Molecular weight of water	kg/kg_{mol}
Nu	Nussult number	-
P	Partial pressure	kPa
Pr	Prandtel number-	

Q	Conduction heat transfer	W/m^2
R	Universal constant	$m^3kPa/kg_{mol}\ K$
Re	Reynolds number	-
t	Time	s
T	Temperature	K
X	Moisture content	kg/kg
T_a	Air Temperature	K
ρ	Density	kg/m^3
Sc	Schmidt number	

Subscripts

a	Dry crust
nz	Glass nozzle
sr	Surface
v	Vapor
w	Wet core

Author details

Abdulaziz Almubarak*

College of Technological Studies, Department of Chemical Engineering, Kuwait

References

[1] Sparrow E, Lin S. Boundary Layer With Prescribed Heat Flux Application to Simultaneous Convective and Radiation. International Journal of Heat and Mass Transfer 1965; 8, 437- 448.

[2] Luikov A. Conjugate Convective Heat Transfer Problems. International Journal of Heat and Mass Transfer 1974; 17, 257-265.

[3] Chyou T. The effect of A Short Unheated Length and A Concentrated Heat Source on The Heat Transfer Through A Turbulent Boundary Layer. International Journal of Heat and Mass Transfer 1991; 34, 1917-1928.

[4] Harris S, Ingham D, Pop I. Transient Boundary Layer Heat Transfer From A Flat Plate Subjected To A Sudden Change in Heat Flux. European Journal of Mechanics B- Fluid 2001; 20, 187-204.

[5] Deswita L, Nazar R, Ahmad R, Ishak A, Pop I. Similarity Solutions of Free Convection Boundary Layer Flow on a Horizontal Plate with Variable Wall Temperature. European Journal of Scientific Research 2009; 27(2) 188-198.

[6] Defraeyea T, Houvenaghelc G, Carmelieta J, Derome D. Numerical Analysis of Convective Drying of Gypsum Boards. International Journal of Heat and Mass Transfer 2012; 55, 4487-4928.

[7] Mori S, Nakagwa H, Tanimoto A, Sakakibara M. Heat and Mass Transfer With A Boundary Layer Flow Past A Flat Plate of Finite Thickness. International Journal of Heat and Mass Transfer 1991; 34, 2899-2909.

[8] Masmoudi W, Prat M. Heat and Mass Transfer Between A Porous Medium and A Parallel External Flow; Application to Drying of Capillary Porous Material. International Journal of Heat and Mass Transfer 1991; 34, 1975-1989.

[9] Jomaa W, Bruneau D, Nadeau J. Simulation of The High Temperature Drying of A Past Product: on The Influence of The Local Air Flow and The Thermal Radiation. Drying Technology 2004; 22, 1709-1729.

[10] Ranz W, Marshall W. Evaporation From Drops. Chemical Engineering Progress 1952; 48, 141-173.

[11] Trommelen A, Crosby E. Evaporation and Drying of Drops in Superheated Vapors. AIChE Journal 1970; 16, 857-872.

[12] Sirignano, W.A. Fluid Dynamics and Transport of Droplets and Sprays: Cambridge University Press, NY, USA 1999.

[13] Masters K. Spray Drying in Practice. Spray Dry Consult International: Denmark: John Wiley & Sons Inc., NY, USA 2002.

[14] Sloth J, Kiil S, Jensen A, Andersen S, Jørgensen K, Schiffter H, Lee G. Model Based Analysis of The Drying of A Single Solution Droplet in An ultrasonic Levitator. Chemical Engineering Science 2006; 61, 2701-2709.

[15] Miura K, Miura T, Ohtani S. Heat and Mass Transfer to and From Droplets. American Journal of Chemical Engineers, Symposium series 1977; 73 (163).

[16] Ali H, Mumford C, Jefferys G., Bains G. A study of evaporation from, and drying of, single droplets. In: Mujumdar AS. (editor) Proceedings of the 6th International Symposium in Drying IDS'88. Versailles, France.1988.

[17] Minoshima H, Matsushima K, Liang H, Shinohara K. Estimation of Diameter of Granule Prepared by Spray Drying of Slurry with Fast and Easy Evaporation. Journal of Chemical Engineering of Japan 2002; 35, 880-885.

[18] Seydel P. Experimental and Mathematical Modeling of Solid Formation at Spray Drying. Chemical Engineering Technology 2004; 27 (5): 505-510.

[19] Perdana J, Fox M, Schutyser M, Boom R. Single-Droplet Experimentation on Spray Drying: Evaporation of a Sessile Droplet. Chemical Engineering & Technology 2011; 34 (7): 1151–1158.

[20] Cheong H, Jeffreys G, Mumford C. A Receding Interface Model For The Drying of Slurry Droplets. AIChE Journal 1986; 32, 1334-1346.

[21] Farid M. A New Approach to Modeling of Single Droplet Drying. Chemical Engineering Science 2003; 58, 2985-2993.

[22] Almubarak A, Mumford C. Characteristics of the receding evaporation front in convective drying. In: Mujumdar AS. (editor) Proceedings of the 9th International Drying Symposium, IDS'94, Marcel Dekker Inc., NY, USA; 1994.

[23] Kays W. M, Crawford M.E. Convective Heat and Mass Transfer, 2nd. ed., McGraw-Hill Book Company, New York, NY, USA.1980.

[24] Thomas L. C. Heat Transfer professional Version. 2nd ed.: Capston Publishing Corporation, OK. USA. 1999.

[25] Kreith F, Bohn M. Principles of Heat Transfer. 6th ed.: Brook/Cole Publishers, Pacific Grove, CA, USA 2001.

[26] Almubarak A, Al-Saeedi J, Shoukry M. Effect of Boundary Layer on Mechanisms of Beach and Desert sand. European Journal of Soil Science 2008; 59, 807-816.

[27] Waananen K, Litchfield J, Okos M. Classification of Drying Models for Porous Solids, Drying Technology 1993; 11, 1-40.

[28] Holman J.P. Heat Transfer: McGraw-Hill Book Co., NY, USA 2002.

[29] Nesic S, Vodnik J. Kinetics of Droplet Evaporation. Chemical Engineering Science 1991; 46, 527-537.

[30] Chen X, Peng F. Modified Biot Number in The Context of Air Drying of Small Moist Porous Objects. Drying Technology 2005; 23, 83-103.

[31] Hayder M, Mumford C. 1993. Mechanisms of Drying of Skin Forming Materials. Drying Technology 1993; 11, 1713-1750.